Temperature coefficients of crystal defects in multicrystalline silicon wafers

Sissel Tind Kristensen[1], Shuai Nie[2], Charly Berthod[1], Rune Strandberg[1], Jan Ove Odden[3], and Ziv Hameiri[2]

[1]University of Agder, Grimstad, Norway
[2]University of New South Wales, Sydney, NSW, Australia
[3]REC Solar Norway, Kristiansand, Norway

Abstract **— This article investigates the influence of crystallographic defects on the temperature sensitivity of multicrystalline silicon wafers. The thermal characteristics of the implied open circuit voltage is assessed since it determines most of the total temperature sensitivity of the material. Spatially resolved temperature dependent analysis is performed on wafers from various brick positions; intragrain regions, grain boundaries, and dislocation clusters are examined. The crystal regions are studied before and after subjecting the wafers to phosphorus gettering, aiming to alter the metallic impurity concentration in various regions across the wafers. Most intragrain regions and grain boundaries are found to show similar thermal characteristics before gettering. The gettering process has no substantial effect on the temperature sensitivity of intragrain regions, whereas it increases the sensitivity of most grain boundaries. Dislocation clusters exhibit both highest and lowest temperature sensitivities compared with other crystal regions before and after gettering. Images of the recombination parameter γ are created and related to the temperature sensitivity of the Shockley-Read-Hall (SRH) lifetime of the impurities in the material. The results suggest that most intragrain regions and grain boundaries are limited by SRH centers with a modest lifetime**

temperature sensitivity in the studied temperature range. Dislocation clusters are found to contain recombination centers with an effective lifetime that has a beneficial temperature sensitivity. The gettering process is observed to alter the composition of the recombination centers in the dislocation clusters, resulting in an SRH lifetime with an even more favorable temperature sensitivity for most clusters.

G.I. Introduction

Solar cells are usually characterized and optimized under standard test conditions (STC), defined as a global standard solar spectrum AM1.5G, an irradiance of $1000\,\mathrm{W/m^2}$ and a cell temperature of $25\,^{\circ}\mathrm{C}$ [1]. However, real operating temperatures can differ considerably from STC depending on the climate at the location of the installed device [2–4].

The characteristics of solar cells are significantly influenced by the operating temperature as has been studied for decades [4–7]. This causes the performance of most cell types to decrease linearly with increasing temperature [4]. Understanding the performance of solar cells under non-STC is therefore essential to accurately forecast the power production of photovoltaic (PV) installations and to optimize solar cells for different climatic conditions.

The temperature dependence of a solar cell is mainly determined by the temperature sensitivity of the open circuit voltage (V_{oc}). It accounts for approximately $80-90\,\%$ of the total temperature sensitivity of a device which is not constrained by resistance or other fill factor losses [8]. The V_{oc} decreases with increasing temperature due to a reduction of the band gap energy (E_{g}) which consequently increases the intrinsic carrier concentration (n_i) [8–10].

The temperature sensitivity of the V_{oc} can be quantified using the temperature coefficient ($\beta_{V_{\mathrm{oc}}}$) which is a measure of the rate of change in V_{oc} with temperature. In absolute form, and to the first-order approximation, it is given as [11]

$$\beta_{V_{\mathrm{oc}}} = \frac{dV_{\mathrm{oc}}}{dT_{\mathrm{c}}} = -\frac{E_{\mathrm{g0}}/q - V_{\mathrm{oc}} + \gamma k T_{\mathrm{c}}/q}{T_{\mathrm{c}}} \tag{G.1}$$

where E_{g0} denotes the semiconductor bandgap energy extrapolated to $0\,\mathrm{K}$, q is the elementary charge, k is the Boltzmann constant, and T_{c} is the cell temperature. The parameter γ includes the temperature dependence of several parameters determining the dark saturation current, J_0. It can be correlated to physical quantities through [12]

$$\gamma = 1 - \frac{d\ln ERE_{\mathrm{oc}}}{d\ln T_{\mathrm{c}}} + \left(2\frac{d\ln E_{\mathrm{g}}}{d\ln T_{\mathrm{c}}} - \frac{d\ln J_{\mathrm{sc,1sun}}}{d\ln T_{\mathrm{c}}}\right) \tag{G.2}$$

where ERE_{oc} denotes the external radiative efficiency at open circuit condition and $J_{\mathrm{sc,1sun}}$ is the short circuit current density at 1 Sun. The ERE is defined as "the fraction of total

dark saturation current in the device that results in radiative emission from the device" [13]. Eq. (G.2) is mainly determined by the first two terms, meaning that γ contains information about the dominant recombination mechanism in the material. According to Ref. [6], γ usually takes values between 1 and 4 but other, including negative values, have been observed experimentally in recent studies [14–17].

From Eq. (G.1), an approximately linear relationship is predicted between the temperature sensitivity and the material quality. This indicates that a cell with a high V_{oc} will have the inherent advantage of reduced temperature sensitivity. However, $\beta_{V_{\mathrm{oc}}}$ can be significantly influenced by the last term in Eq. (G.1) containing the γ parameter [12]. As an example, it accounted for up to 10 % of the $\beta_{V_{\mathrm{oc}}}$ for the cells mentioned in Ref. [12].

In recent years, increased attention has been given to the influence of crystallographic defects on the temperature sensitivity of silicon wafers and solar cells [14, 16–20]. Eberle *et al.* reported increased temperature sensitivity of V_{oc} in contaminated regions of multicrystalline silicon (mc-Si) cells, but reduced temperature sensitivity for areas containing dislocation clusters [14]. This was further investigated by Eberle *et al.* in a following study, reporting reduced temperature sensitivity of dislocation clusters of mc-Si wafers and cells [18]. The authors suggested that it could be caused by the presence of impurities in the clusters and thus impacted by Shockley-Read-Hall (SRH) recombination. Additionally, more recent studies have reported reduced temperature sensitivity in some dislocation clusters of mc-Si wafers and cells and identified advantageous thermal behavior of wafers originating from the top of the bricks [16, 17, 19–21]. These findings illustrate the importance of further studies to evaluate the varying influence of different defect types on the temperature sensitivity of V_{oc}.

This study investigates the influence of crystal defects on the temperature sensitivity of mc-Si wafers. The temperature coefficient of the implied V_{oc} ($\beta_{iV_{\mathrm{oc}}}$) is assessed for intra-grain regions, grain boundaries, and dislocation clusters on wafers from various brick positions. The crystal areas are examined before and after being subjected to phosphorus diffusion gettering (PDG) which is known to alter the concentration of metallic impurities across the wafers [22–26], thus, enabling an investigation of how the temperature sensitivity is influenced by metallic impurities.

G.II. Experimental Method

A. Sample Preparation

The wafers were fabricated from a high-performance (HP) *p*-type mc-Si ingot, tri-doped with boron, gallium and phosphorus. The ingot was produced from a blend of compensated silicon [Elkem Solar Silicon® (ESS®)] and polysilicon with a blend-in-ratio of 70 %

ESS® and targeted resistivity of 0.9 Ω·cm (produced in 2015). Doping and resistivity profiles of the ingot can be found in Ref. [27]. Seven 6" wafers were then chosen from a central brick, originating from different positions from the bottom to the top of the brick.

The wafers were processed in two steps: Step 1 (referred to as *ungettered*): The as-sawn wafers received saw damage etching (final thicknesses: 194 μm $\pm$ 7 μm), cleaning [28], and passivation with 75 nm silicon nitride (SiN_x) using an industrial plasma-enhanced chemical vapor deposition (PECVD) system (MAiA, Meyer Burger) at a deposition temperature of 400 °C [29]. Step 2 (referred to as *gettered*): The passivation from Step 1 was removed using hydrofluoric (HF) acid followed by a second clean. A conventional PDG [26] was performed by subjecting the wafers to a 45 min $POCl_3$ diffusion treatment with a peak temperature of 850 °C resulting in a sheet resistance of approximately 40 Ω·cm [30, 31]. The surface gettering layer was then removed by alkali etching and the wafers were re-passivated using an identical SiN_x process as in Step 1. The wafers were fully characterized after Step 1 and after Step 2 in order to study the effect of the PDG process.

B. Characterization

The wafers were characterized using our novel temperature dependent photoluminescence (PL) imaging system [32], enabling acquisition of PL images at elevated temperatures, and subsequently, calibration of the acquired images into spatially resolved maps of effective carrier lifetime (τ_{eff}), implied V_{oc} (iV_{oc}), $\beta_{iV_{\text{oc}}}$, and γ. The PL images were obtained at a photon flux of $1.2 \cdot 10^{17}\,\text{cm}^{-2}\text{s}^{-1}$, corresponding to an illumination intensity of approximately 0.5 Sun (the highest that can be achieved with our current setup). The images were acquired at 25 °C and 70 °C. These two temperatures are assumed to give a valid representation of the temperature dependence of iV_{oc}, since mc-Si cell parameters usually vary linearly with temperature for normal operating temperatures [8]. The validity of this assumption was confirmed by obtaining PL images of one wafer at temperatures ranging from 25 °C to 70 °C in steps of 10 °C.

The PL images of the ungettered wafers were calibrated using a temperature dependent photo-conductance (PC) signal directly measured on a region of the wafer during the PL image acquisition. A detailed description of the calibration procedure can be found in Ref. [32]. The PL images of the gettered wafers were calibrated using a novel temperature dependent PL-based detection to account for trapping observed for these wafers at relevant injection levels [33]. The calibration was performed using injection dependent τ_{eff} curves obtained by simultaneously measuring PC and PL signals on the wafer. First, the τ_{eff} curves were matched at high injection (as the PC signal is not impacted by traps at high injection), then the PL images were calibrated using the PL-based τ_{eff}. A detailed description of the calibration procedure can be found in Ref. [20]. The wafers before and

after gettering were, therefore, both calibrated using PC-based measurements enabling a meaningful comparison. A sensitivity function was implemented to account for the local sensitivity profile of the PC sensor (measured according to Ref. [34]). Additionally, the doping densities from Ref. [27] and the mobility model for compensated Si were implemented in the calibration [35]. The temperature dependence of the surface recombination is assumed be negligible in the studied temperature range following Ref. [36]. After the elevated temperature measurements, τ_{eff} curves of the samples were obtained at 25 °C using a Sinton WCT-120 (Sinton Instruments) to ensure that no permanent annealing effects occurred.

C. Analysis

Examples of calibrated PL images are given in Figs. G.1(a) and (b) showing spatially resolved iV_{oc} at 25 °C before and after gettering. An image of absolute $\beta_{iV_{\text{oc}}}$ can be obtained from the calibrated iV_{oc} image by applying

$$\beta_{iV_{\text{oc,abs},xy}} = \frac{iV_{\text{oc},T2,xy} - iV_{\text{oc},T1,xy}}{T_2 - T_1}, \tag{G.3}$$

to each pixel, as is illustrated in Figs. G.1(d) and (e). Images of relative $\beta_{iV_{\text{oc}}}$ can be obtained by normalizing each pixel with the local iV_{oc} at 25 °C (not shown). Finally, maps of γ can be created by applying Eq. (G.1) to each pixel [see for example Figs. G.5(b) and (c)]. A circular heat stage (Sinton WCT-120TS, diameter of 150 mm) was used for imaging, causing both inhomogeneous wafer temperature and reflection outside of the heat stage. Therefore, only the areas with uniform temperature and reflection are used for further analysis. Different regions were selected on each wafer containing either intra-grain regions, grain boundaries, or dislocation clusters, to study the temperature sensitivity before and after PDG. Several regions of the same crystal type were investigated on each wafer to monitor the representativeness of the results. Examples of the selected regions of interest (ROIs) for (A) an intra-grain region, (B) a dislocation cluster, and (C) a grain boundary are illustrated by squares in Fig. G.1(b). Note that the actual ROI C is chosen so that only one grain boundary is selected and is therefore smaller than shown in the figure.

G.III. Results and Discussion

A. Spatially Resolved Temperature Sensitivity

To illustrate some general temperature related characteristics, Fig. G.1 presents spatially resolved images of iV_{oc} at 25 °C and $\beta_{iV_{\text{oc}}}$ of a wafer from the middle of the brick before

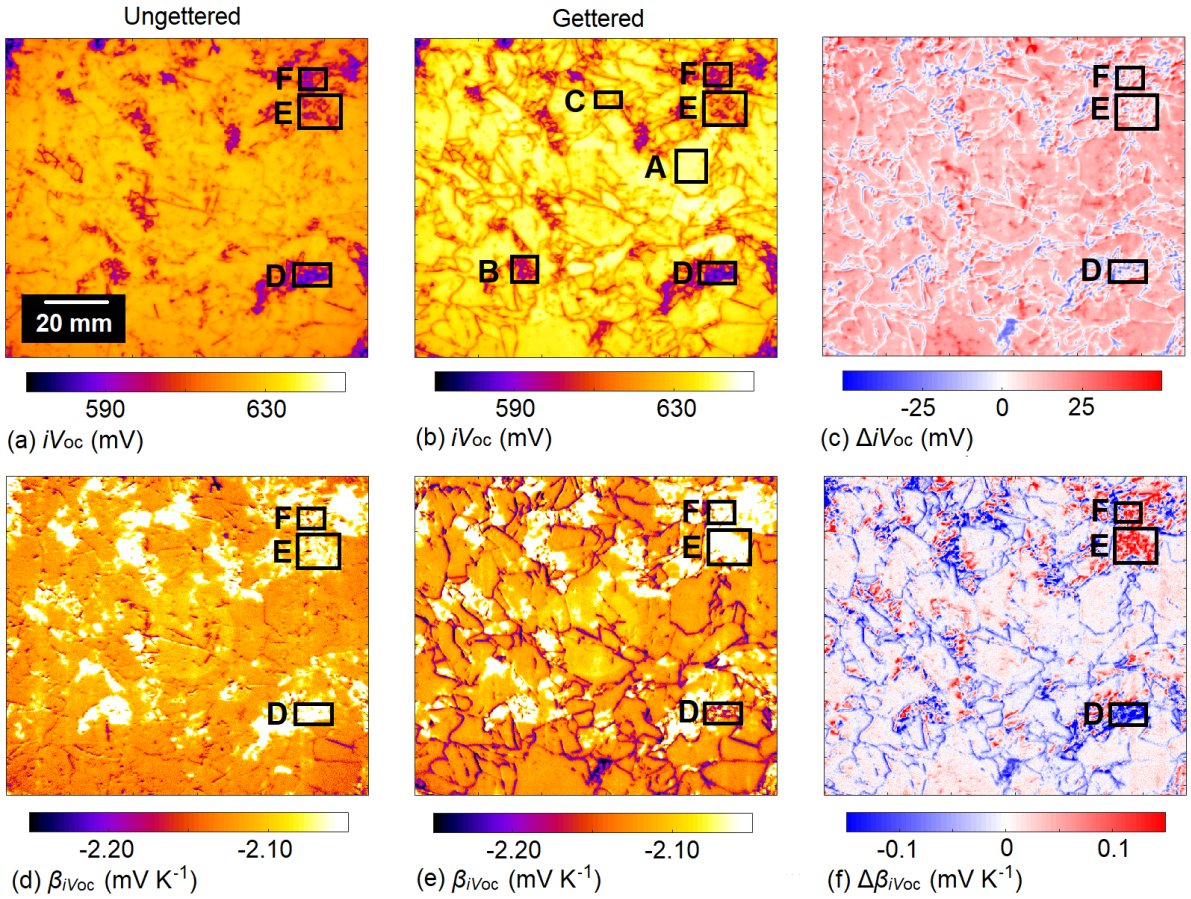

Figure G.1: Spatially resolved images of iV_{oc} at 25 °C and $\beta_{iV_{\mathrm{oc}}}$ before (a,d) and after (b,e) gettering for a wafer from the middle of the brick, and spatially resolved images of ΔiV_{oc} (c) and $\Delta\beta_{iV_{\mathrm{oc}}}$ (f).

and after PDG. Recombination active grain boundaries appear as dark lines in the images and dislocations appear as dark clusters. Figs. G.1(a) and (b) show images of iV_{oc} of the wafer before and after PDG, respectively. In the ungettered state, the intra-grain regions and most grain boundaries are found to exhibit similar material quality. Dislocation clusters appear recombination active in this state, as also reported in Ref. [23]. After PDG, the quality of the intra-grain regions is improved, suggesting that PDG is successful in reducing the concentration of detrimental metallic impurities in these areas. Similar observations have been made in Refs. [22,26]. The recombination activity of most of the grain boundaries increases with gettering, similar to what has been reported by for example Refs. [22, 23, 37]. The activation and increased recombination strength of grain boundaries during PDG has been suggested to result from metal decoration of the structures causing a change in recombination behavior [24, 37–39]. Dislocations continue to be recombination active after gettering.

To illustrate further the variations in iV_{oc} observed across the wafer, an image of the

change in iV_{oc} is created by applying $\Delta iV_{oc} = iV_{oc}(\text{gettered}) - iV_{oc}(\text{ungettered})$ to each pixel. This is shown in Fig. G.1(c). The improvement of the intra-grain regions and the reduced quality of the grain boundaries are clearly visible. Additionally, Fig. G.1(c) illustrates how several dislocation clusters experience increased recombination strength from PDG, similar to observations made in Ref. [23].

Turning our attention to the temperature sensitivity, spatially resolved images of $\beta_{iV_{oc}}$ are presented in Figs. G.1(d) and (e) for the wafer before and after PDG, respectively. The intra-grain regions and grain boundaries are found to show a similar thermal behavior in the ungettered state. From Fig. G.1(d), features with low temperature sensitivity (bright areas) can be observed across the wafer [see for example ROIs D-F]. Comparing the images of iV_{oc} and $\beta_{iV_{oc}}$, the bright features can be correlated with dislocation clusters. The relationship between dislocation clusters and low temperature sensitivity has been observed experimentally in recent studies [14, 16, 18–20, 32]; however, note that a region with low iV_{oc} is theoretically expected to show high temperature sensitivity for a constant γ, following Eq. (G.1).

After PDG, the temperature sensitivity of the intra-grain regions is not substantially affected despite of the increase in material quality. This will be assessed further in Sec. G.III.B. The grain boundaries are found to exhibit increased temperature sensitivity after gettering as a result of the direct relationship between material quality and temperature coefficients presented in Eq. (G.1). Features with low temperature sensitivity (bright areas) can be observed across the wafer and correlated with dislocation clusters, similar to the observations in the ungettered state. Since this observation applies both before and after PDG, it suggests that the cause for the low temperature sensitivity is not removed by the gettering process. Although most dislocation clusters show low temperature sensitivity, there are also some that exhibit high temperature sensitivity. This is illustrated by ROIs D-F, highlighted on all images in Fig. G.1. All three dislocation clusters exhibit lower temperature sensitivity compared to the rest of the wafer before gettering [Fig. G.1(d)]. However, after gettering, ROI D displays higher temperature sensitivity, while ROIs E and F remain as low temperature sensitivity regions [Fig. G.1(e)]. Similar observations have been made for non-compensated p-type Si wafers treated by similar gettering and passivation processes [20], suggesting that our results can be generalized to non-compensated mc-Si.

To illustrate further the different responses to gettering across the wafer, a map of the change in $\beta_{iV_{oc}}$ is created by applying $\Delta\beta_{iV_{oc}} = \beta_{iV_{oc}}(\text{gettered}) - \beta_{iV_{oc}}(\text{ungettered})$ to each pixel, as shown in Fig. G.1(f). Fig. G.1(f) clearly illustrates the increased temperature sensitivity of the grain boundaries and the small altering of the intra-grain regions. Perhaps surprisingly, the dislocation clusters, and even parts of clusters, show very different

changes in $\beta_{iV_{oc}}$. Both relatively large increase and decrease in temperature sensitivity can be observed across the wafer, as indicated by the ROIs D-F. The root cause of this will be investigated further in Secs. G.III.D and G.III.E.

It should be noted that further processing, such as firing and metallization, may have a large impact on the temperature sensitivity due to hydrogenation from the SiN_x and modified lateral conduction in the sample [20]. However, studies have shown beneficial $\beta_{iV_{oc}}$ values in dislocation clusters both before and after firing and metallization [18, 20].

B. Intra-grain Regions

Fig. G.1 clearly illustrates the varying gettering response of different regions. Additionally, literature has shown that brick position can have a significant impact on the recombination activity of different crystal defects in the as-grown state and, consequently, how they respond to gettering [23, 26]. A detailed investigation of intra-grain regions, grain boundaries, and dislocation clusters, and the position of the wafer in the brick, is therefore presented.

Five intra-grain regions are randomly selected on each wafer following the procedure described in Sec. G.II.C, and the average temperature sensitivity of the different regions is assessed. This is illustrated in Fig. G.2(a) showing the variations in average iV_{oc} at 25 °C in each selected region as a function of the relative brick height before and after gettering. The error bars denote the minimum and maximum average values. The average iV_{oc} is found to increase for most of the wafers as a result of the gettering process, however, this increase is most prominent in the bottom and towards the top of the brick. It suggests that PDG is effective in removing metallic impurities from the intra-grain regions, especially for wafers from these brick locations, similar to observations made in Refs. [22, 26]. This is likely to be caused by the higher concentration of impurities typically found in the bottom and towards the top of a mc-Si brick, thus, enabling more effectful gettering. The higher concentration of impurities is typically a result of segregation during solidification and in-diffusion of impurities from the crucible [40, 41].

Fig. G.2(d) shows average $\beta_{iV_{oc}}$ values of the selected intra-grain regions as a function of brick height before and after gettering. The variation in average temperature sensitivity on each wafer is found to be relatively small, however, some variations are observed along the brick. There is no clear indication that removing metallic impurities from the intra-grain areas improves the temperature sensitivity.

An illustration of the distribution of $\beta_{iV_{oc}}$ values in the intra-grain regions before and after gettering is presented in Figs. G.3(a), (d) and (g). It shows $\beta_{iV_{oc}}$ as a function of iV_{oc} at 25 °C for each pixel in selected intra-grain areas from wafers from the bottom, middle and top of the brick. Lines are inserted in the figure to illustrate the theoretical

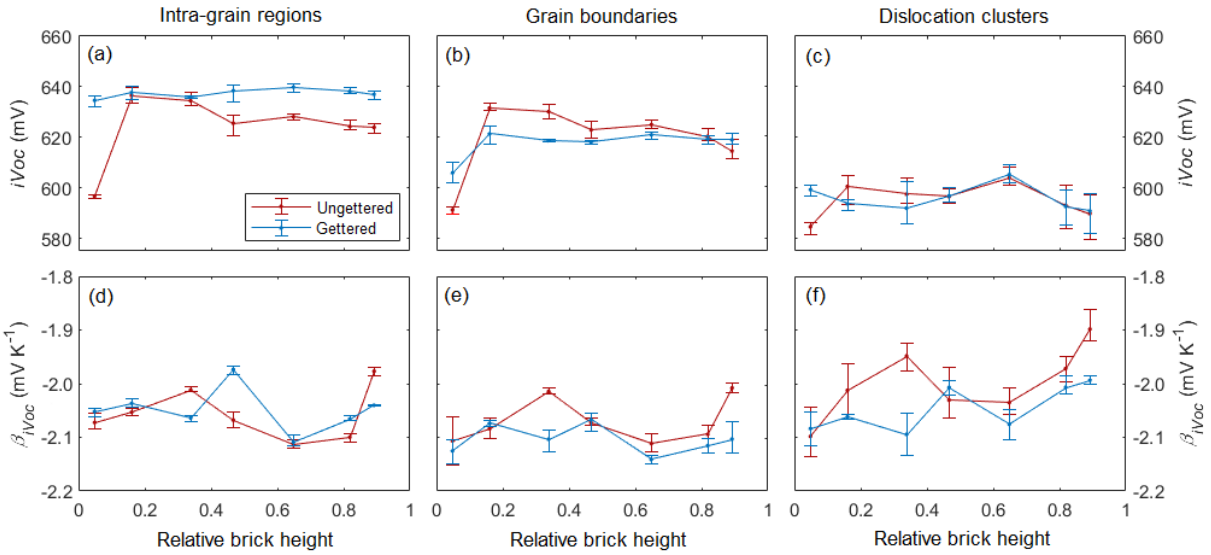

Figure G.2: Average iV_{oc} at 25 °C and $\beta_{iV_{\mathrm{oc}}}$ values of selected intra-grain regions, grain boundaries and dislocation clusters as a function of relative brick height before and after gettering. The error bars denote minimum and maximum average values in the selected areas.

relationship between temperature sensitivity and material quality for constant γ values, calculated from Eq. (G.1). The spread in $\beta_{iV_{\mathrm{oc}}}$ and iV_{oc} within each region is found to be relatively small (note that the number of pixels in each selected area is in the same range as the dislocation clusters for the respective brick positions [500-800 pixels, see Fig. G.3(c) for comparison]. The temperature sensitivity is not substantially affected by the gettering process even though the regions experience increased iV_{oc} values. All intra-grain regions show an increased iV_{oc} as a result of gettering. The shift in $\beta_{iV_{\mathrm{oc}}}$ and iV_{oc} follows the iso-γ line for the middle wafer. The intra-grain regions on the wafers from the bottom and the top of the brick shift towards higher γ values. This difference observed for various brick positions could be caused by the higher concentration of metallic impurities in the bottom and top of the brick, resulting in a more substantial altering of the recombination processes in these regions. Interestingly, all intra-grain regions take values near the same theoretical line given by $\gamma = 3$ after gettering.

C. Grain Boundaries

Figs. G.2(b) and (e) show average values of iV_{oc} at 25 °C and $\beta_{iV_{\mathrm{oc}}}$ of five randomly selected grain boundaries on each wafer as a function of brick height before and after gettering. The average iV_{oc} values are comparable with intra-grain regions before gettering. This is consistent with observations made in Fig. G.1(a) where most grain boundaries and intra-grain areas were found to display similar material quality. After gettering, the

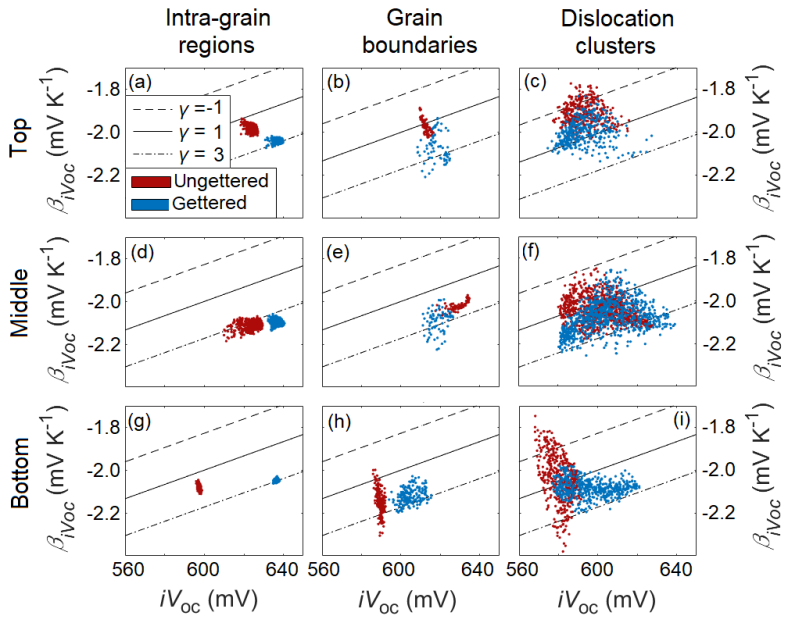

Figure G.3: Pixel resolution of $\beta_{iV_{oc}}$ as a function of iV_{oc} at 25 °C in an intra-grain region, grain boundary and dislocation cluster from wafers from the bottom, middle, and top of the brick.

average iV_{oc} values of the grain boundaries decrease for wafers from the middle of the brick. The decrease in material quality is likely to result from metal decoration of the grain boundaries [22–24, 37–39]. The bottom wafer experiences an increase in average iV_{oc} after gettering. By assessing the corresponding PL images, the grain boundaries of this wafer were found to be recombination active both in the ungettered and gettered state. Similar observations have been made in Ref. [22] for an industrial HP mc-Si brick. The average $\beta_{iV_{oc}}$ decreases (more negative) for most brick positions in agreement with the direct relationship between material quality and temperature coefficients for constant γ, presented in Eq. (G.1). The two bottom wafers show no significant change in $\beta_{iV_{oc}}$ since the grain boundaries are already recombination active in the ungettered state. Comparing to intra-grain regions, the temperature sensitivity of grain boundaries is higher after gettering for most brick positions.

An illustration of the distribution of $\beta_{iV_{oc}}$ values in the grain boundaries before and after gettering is given in Figs. G.3(b), (e) and (h). They show $\beta_{iV_{oc}}$ as a function of iV_{oc} at 25 °C for each pixel in selected grain boundaries on wafers from the bottom, middle and top of the brick. The gettering process is found to significantly scatter $\beta_{iV_{oc}}$ and iV_{oc}. The middle and top wafers show a clear increase in temperature sensitivity and additionally, a shift in γ. The bottom wafer shows relatively high temperature sensitivity both before and after gettering despite of an improvement in iV_{oc}. The gettering response of the grain boundaries varies for the different brick positions; however, it is worth noticing that the

gettering process shifts the pixel values towards an iso-γ line with $\gamma = 3$. This observation is similar to the γ values found for intra-grain regions after gettering despite of different $\beta_{iV_{\mathrm{oc}}}$ values found for the two crystal types. This will be discussed further in Sec. G.III.E.

D. Dislocation Clusters

Figs. G.2(c) and (f) show average iV_{oc} at 25 °C and $\beta_{iV_{\mathrm{oc}}}$ values of five randomly selected dislocation clusters as a function of brick height before and after gettering. The spread in average values of both iV_{oc} and $\beta_{iV_{\mathrm{oc}}}$ is considerably larger than for intra-grain regions and grain boundaries. This is consistent with observations from Fig. G.1 illustrating how different dislocation clusters can exhibit significant variations in temperature sensitivity before and after gettering, even across individual wafers. As expected, the average iV_{oc} values are substantially lower than the ones found for both intra-grain regions and grain boundaries before and after gettering, indicating recombination active dislocation clusters in both states. For some clusters and brick positions, iV_{oc} is not significantly influenced by PDG; but the temperature sensitivity increases. It is worth noticing that dislocation clusters show considerably lower average temperature sensitivity towards the top of the brick compared to the intra-grain areas and grain boundaries. This suggests that dislocation clusters from the top of the brick have unique properties which make a temperature increase less detrimental to the performance.

Figs. G.3(c), (f), and (i) illustrate $\beta_{iV_{\mathrm{oc}}}$ as a function of iV_{oc} at 25 °C for each pixel within selected regions on wafers from the bottom, middle, and top of the brick. Each dislocation cluster is found to show a large spread in the values of iV_{oc} and $\beta_{iV_{\mathrm{oc}}}$, both before and after gettering, compared to the intra-grain regions and grain boundaries. Interestingly, some pixels in the dislocation clusters show very low temperature sensitivity compared to the other crystal regions. Additionally, the top wafer clearly shows a lower sensitivity compared to clusters from other brick positions. The distribution of $\beta_{iV_{\mathrm{oc}}}$ values in the selected dislocation clusters is shifted towards higher temperature sensitivity by PDG. The shifts do not follow the theoretical iso-γ lines. It should be stressed that other dislocation clusters might be affected differently by PDG.

From results presented so far, dislocations show a complex response to gettering and a complex thermal behavior. Nonetheless, the regions across the wafers with low temperature sensitivity can still be correlated with dislocation clusters both before and after gettering. It is therefore interesting to investigate further the properties that characterize clusters showing low temperature sensitivity and distinguish them from clusters displaying increased sensitivity. This is done by revisiting Fig. G.1, presenting spatially resolved images of iV_{oc} and $\Delta\beta_{iV_{\mathrm{oc}}}$ for the wafer originating from the middle of the brick. Three ROIs are marked on the wafer (D-F), highlighting three dislocation clusters with different

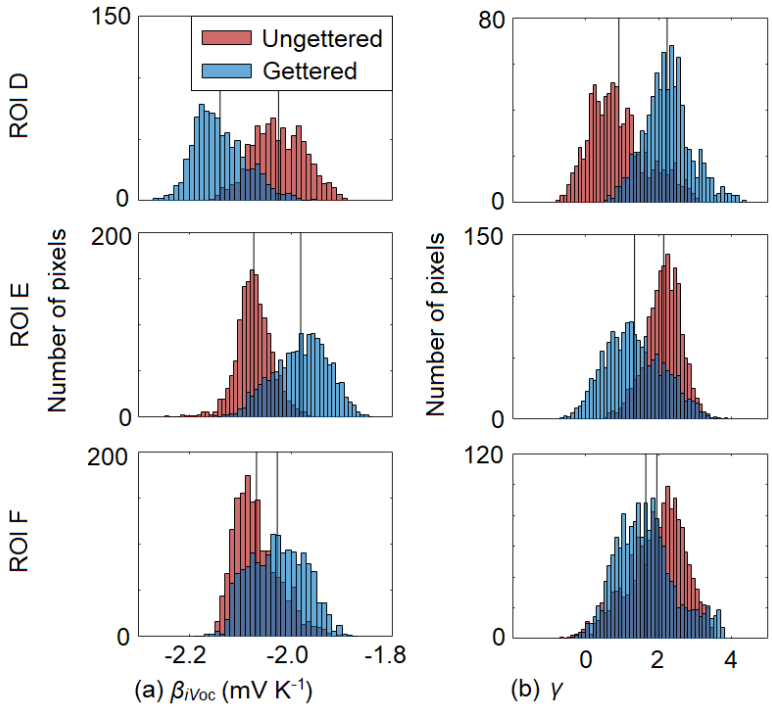

Figure G.4: Distribution of $\beta_{iV_{oc}}$ (a) and γ (b) of three dislocation clusters marked by ROIs D-F on Fig. G.1. Average values are indicated by black lines in the histograms.

responses to gettering. ROI D exhibits increased temperature sensitivity after PGD, while ROIs E and F exhibit reduced sensitivity. The actual distributions of $\beta_{iV_{oc}}$ and γ values in the clusters before and after gettering are presented in Figs. G.4(a) and (b). Average values are indicated by black lines in the histograms and summarized in Table G.1. All dislocation clusters experience a shift in γ as a result of the gettering process; however, ROIs E and F experience a decrease in γ, where the opposite is observed for ROI D. This implies that the gettering process alters the composition of recombination mechanisms in the clusters, but in various ways depending on the cluster type. From Eq. (G.1), a high γ value contributes to increasing the temperature sensitivity and vice versa. The limiting recombination mechanism therefore becomes more temperature sensitive for ROI D and less sensitive for ROIs E and F as a result of PDG. The physical implications of an increase and decrease in γ will be discussed further in Sec. G.III.E. It is worth noticing that even though some dislocation clusters become more temperature sensitive after gettering, as illustrated in blue in Fig. G.1(e), the temperature sensitivity can still be lower compared to other crystal areas on the wafer.

E. Mapping of Limiting Recombination Mechanisms

Figs. G.1-G.4 illustrate how variations in temperature sensitivity can be observed across wafers and for different brick positions. The temperature sensitivity depends on several

Table G.1: Average γ values of ROIs D-F on a wafer from the middle of the brick before and after gettering.

Processing	ROI D	ROI E	ROI F
Ungettered	0.91	2.14	1.95
Gettered	2.24	1.34	1.65

factors as described in Eq. (G.1), but the material dependent variability is captured by the parameters iV_{oc} and γ. In order to understand the underlaying mechanisms causing varying temperature sensitivity, the γ parameter is assessed in further detail.

To correlate actual γ values with physical quantities, we make the following observations: First, Eq. (G.1) indicates that a low γ value will contribute to lowering the temperature sensitivity, and vice versa. Secondly, we make use of Ref. [4], where Dupré *et al.* compute γ values for different scenarios. These values should not be understood as limits, but as reference points for interpretation. The authors suggest $\gamma \approx 3$ for a material which is limited by SRH recombination in the bulk and at the surface and with carrier lifetime and surface recombination velocities assumed to be independent of temperature. This implies that, for a material which is limited by SRH recombination in the bulk and at the surface, $\gamma < 3$ is equivalent to an effective SRH lifetime that increases with increasing temperature. The actual γ value can then be related to the rate by which the lifetime is increasing. This rate is determined by the energy level of the defect states (E_{t}) and the capture cross sections of electrons (σ_n) and holes (σ_p) [42–44]. It should be noted that other parameters, such as injection level, could influence as well.

Spatially resolved images of γ for wafers from the bottom, middle, and top of the brick are shown before gettering [Figs. G.5(b), (f), and (j)] and after gettering [Figs. G.5(c), (g) and (k)]. Note that a non-uniformity can be observed in the bottom right corner of Fig. G.5(j) originating from a slight non-uniform temperature encountered during the measurement of the ungettered wafer at 70 °C (it should be stressed that this has not been observed for other measurements). The non-uniformity was found to be localized and only the unaffected part of the wafer is used for analysis. Large variations in γ are found across the wafers, especially noticeable for the middle and top wafers. If comparing with corresponding iV_{oc} images [Figs. G.5(a), (e), and (i)], the various crystal regions can be correlated to γ values. Intra-grain regions exhibit a relatively uniform γ value across individual wafers and take a common value around $\gamma = 3$ after gettering, similar to observations from Fig. G.3. Following our previous discussion, this γ value implies that the intra-grain regions are limited by SRH recombination centers with an effective lifetime that is independent of temperature or has a modest temperature sensitivity in the studied temperature range. Such a temperature dependence characterizes, for example,

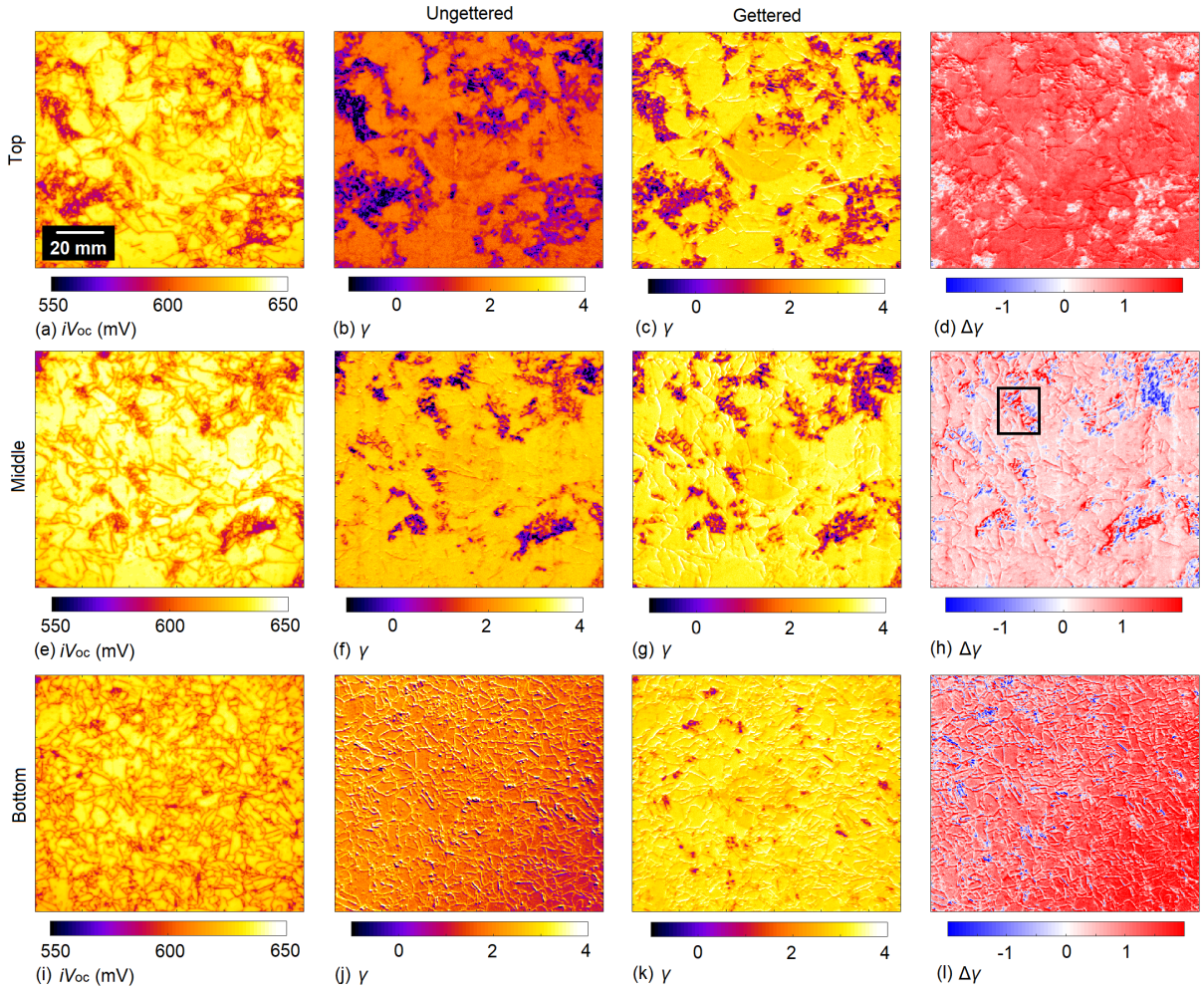

Figure G.5: Images of iV_{oc} at 25 °C after gettering, γ before and after gettering, and $\Delta\gamma$ for wafers from (a-d) the top, (e-h) middle, and (i-l) bottom of the brick.

interstitial iron [18,45,46] suggesting that this SRH center could be limiting the intra-grain regions.

Grain boundaries cannot easily be distinguished from intra-grain regions in the ungettered nor gettered states, except for the bottom wafer. This suggests that grain boundaries and intra-grain regions are limited by the same type of recombination in the middle and top wafers, or by different SRH centers resulting in a similar temperature dependence. Grain boundaries have been observed to show a higher concentration of iron after gettering [24], supporting this hypothesis. Note however, that the intra-grain regions and grain boundaries show very different iV_{oc} and $\beta_{iV_{oc}}$ values after gettering [see Figs. G.2(a) and (b)] indicating different characteristics of the limiting recombination mechanism at the two locations. One possible explanation could be that the two crystallographic groups contain different concentrations of the same SRH center. The visibility of the grain boundaries in the bottom wafer before gettering indicates that this case is characterized

by different types of recombination compared to the other wafers in the ungettered state. The γ parameter could be influenced by in-diffused impurities from the crucible during solidification. This hypothesis is supported by the very low iV_{oc} values encountered for this wafer.

Features with low, and in some cases negative, γ values can be observed across both the ungettered and gettered wafers and correlated with dislocation clusters when compared with the iV_{oc} images. The low γ values observed in dislocation clusters indicate that the clusters contain SRH centers with an effective lifetime that has an especially beneficial temperature sensitivity. Examples of such SRH centers could be copper [47], aluminum [48], molybdenum [45, 49], titanium [50] and chromium-related defects [18, 51].

To illustrate more clearly how PDG affects the various crystal regions, images of $\Delta\gamma$ are calculated by applying $\Delta\gamma = \gamma(\text{gettered}) - \gamma(\text{ungettered})$ to each pixel. Local variations in γ indicate a change in the limiting recombination type caused by a local redistribution of recombination centers. For $\Delta\gamma < 0$, the redistribution results in a combined recombination rate which becomes less temperature sensitive, and vice versa. Images of $\Delta\gamma$ of wafers from the top, middle, and bottom of the brick can be seen in Figs. G.5(d), (h), and (l). It is clearly visible that γ of intra-grain regions is increased by PDG for all the wafers, however, only a modest change is observed for the middle wafer. The common reaction to PDG by the bottom and top wafer could be caused by the higher concentration of impurities present in these parts of the brick before gettering as a result of in-diffusion from the crucible in the bottom of the brick and segregation of impurities towards the top of the brick. Since the wafers exhibit $\Delta\gamma > 0$, the lifetime of the impurities which are removed by the gettering process have a lower temperature sensitivity than the ones remaining. Dislocation clusters mainly exhibit $\Delta\gamma < 0$; however, some clusters show both a high increase and decrease in γ [see the ROI marked in Fig. G.5(h) as an example]. The variation in γ indicates a rearrangement of recombination centers in clusters. For most dislocation clusters, this rearrangement results in limiting recombination centers yielding a more beneficial temperature sensitivity.

The reduced temperature sensitivity found for most dislocation clusters, compared to intra-grain areas and grain boundaries, indicates that the presence of dislocation clusters may contribute to a beneficial temperature sensitivity of the overall cell performance. Hence, despite their detrimental effect on cell performance, the presence of dislocation clusters might have less harmful effects when the operating temperatures are high.

G.IV. Summary

The temperature sensitivity of crystallographic defects in mc-Si wafers has been investigated. Spatially resolved temperature dependent analysis has been performed on mc-Si

wafers from different brick positions; and intra-grain regions, grain boundaries, and dislocation clusters were examined before and after subjecting the wafers to a phosphorus diffusion gettering. Both intra-grain regions and grain boundaries were found to show similar thermal characteristics before gettering. The gettering process had no substantial effect on the temperature sensitivity of intra-grain regions but increased the sensitivity of most grain boundaries. Dislocation clusters were observed to exhibit both highest and lowest temperature sensitivity compared to other crystal regions.

Images of the recombination parameter γ were created and related to the temperature sensitivity of the local effective lifetime of the SRH centers in the material. The results suggest that most intra-grain regions and grain boundaries are limited by SRH centers with a modest lifetime temperature sensitivity in the studied temperature range such as interstitial iron. Dislocation clusters were found to contain SRH centers with an effective lifetime that has a beneficial temperature sensitivity. The gettering process was found to alter the composition of recombination centers in the clusters, resulting in a SRH lifetime with a more favorable temperature sensitivity for most clusters.

Acknowledgments

This work was supported by the Australian Government through Australian Renewable Energy Agency (ARENA; project 2017/RND001). The views expressed herein are not necessarily the views of the Australian Government, and the Australian Government does not accept responsibility for any information or advice contained herein. The authors thank the Solar Industry Research Facility (SIRF) team at UNSW for samples fabrication.

Bibliography

[1] IEC, "Photovoltaic Devices - Part 1-10, IEC 60904," 2009.

[2] D. Moser, M. Pichler, and M. Nikolaeva-Dimitrova, "Filtering procedures for reliable outdoor temperature coefficients in different photovoltaic technologies," *AMSE. J. Sol. Energy Eng.*, vol. 136, no. 2, pp. 021006-1-10, 2014.

[3] S. Kurtz, K. Whitfield, G. TamizhMani, M. Koehl, D. Miller, J. Joyce, J. Wohlgemuth, N. Bosco, M. Kempe, and T. Zgoena, "Evaluation of high-temperature exposure of photovoltaic modules," *Prog. Photovolt: Res. Appl.*, vol. 19, pp. 954-965, 2011.

[4] O. Dupré, R. Vaillon, and M. A. Green, *Thermal Behavior of Photovoltaic Devices: Physics and Engineering*, Cham, Switzerland: Springer, 2017.

[5] J. J. Wysocki and P. Rappaport, "Effect of temperature on photovoltaic solar energy conversion," *J. Appl. Phys.*, vol. 31, p. 571, 1960.

[6] M. A. Green, *Solar Cells: Operating Principles, Technology, and System Applications*, Englewood Cliffs, N. J.: Prentice-Hall, 1982.

[7] J. C. C. Fan, "Theoretical temperature dependence of solar cell parameters," *Sol. Cells*, vol. 17, pp. 309-315, 1986.

[8] M. A. Green, "General temperature dependence of solar cell performance and implications for device modelling," *Prog. Photovolt: Res. Appl.*, vol. 11, pp. 333-340, 2003.

[9] P. Löper, D. Pysch, A. Richter, M. Hermle, S. Janz, M. Zacharias, and S. W. Glunz, "Analysis of the temperature dependence of the open-circuit voltage," *Energy Procedia*, vol. 27, pp. 135-142, 2012.

[10] H. Steinkemper, I. Geisemeyer, M. C. Schubert, W. Warta, and S. W. Glunz, "Temperature-dependent modeling of silicon solar cells-Eg, ni, recombination, and VOC," *IEEE J. Photovolt.*, vol. 7, pp. 450-457, 2017.

[11] M. A. Green, K. Emery, and A. W. Blakers, "Silicon solar cells with reduced temperature sensitivity," *Electron. Lett.*, vol. 18, no. 2, pp. 97-98, 1982.

[12] O. Dupré, R. Vaillon, and M. A. Green, "Physics of the temperature coefficients of solar cells," *Sol. Energy Mater. Sol. Cells*, vol. 140, pp. 92-100, 2015.

[13] M. A. Green, "Radiative efficiency of state-of-the-art photovoltaic cells," *Prog. Photovolt: Res. Appl.*, vol. 20, pp. 472-476, 2012.

[14] R. Eberle, S. T. Haag, I. Geisemeyer, M. Padilla, and M. C. Schubert, "Temperature coefficient imaging for silicon solar cells," *IEEE J. Photovolt.*, vol. 8, no. 4, pp. 930-936, 2018.

[15] O. Dupré, R. Vaillon, and M. A. Green, "Experimental assessment of temperature coefficient theories for silicon solar cells," *IEEE J. Photovolt.*, vol. 6, no. 1, pp. 56-60, 2016.

[16] S. Nie, S. T. Kristensen, A. Gu, and T. Trupke, "A novel method for characterizing temperature sensitivity of silicon wafers and cells," in: *46th IEEE Photovoltaic Specialists Conference*, Chicago, IL, 2019.

[17] S. T. Kristensen, S. Nie, C. Berthod, R. Strandberg, J. O. Odden, and Z. Hameiri, "How gettering affects the temperature sensitivity of the implied open circuit voltage of multicrystalline silicon wafers," in: *46th IEEE Photovoltaic Specialists Conference*, Chicago, IL, 2019.

[18] R. Eberle, A. Fell, S. Mägdefessel, F. Schindler, and M. C. Schubert, "Prediction of local temperature-dependent performance of silicon solar cells," *Prog. Photovolt: Res. Appl.*, vol. 27, pp. 999-1006, 2019.

[19] C. Berthod, S. T. Kristensen, R. Strandberg, J. O. Odden, S. Nie, Z. Hameiri, and T. O. Sætre, "Temperature sensitivity of multicrystalline silicon solar cells," *IEEE J. Photovolt.*, vol. 9, pp. 957-964, 2019.

[20] S. Nie, S. T. Kristensen, A. Gu, R. L. Chin, T. Trupke, and Z. Hameiri, "Photoluminescence-based spatially resolved temperature coefficient maps of silicon wafers and solar cells," *IEEE J. Photovolt.*, in press, pp. 1-12, 2019. DOI: 10.1109/JPHOTOV.2019.2956261.

[21] C. Berthod, R. Strandberg, and J. O. Odden, "Temperature coefficients of compensated silicon solar cells-influence of ingot position and blend-in-ratio," *Energy Procedia*, vol. 77, pp. 15-20, 2015.

[22] H. C. Sio, S. P. Phang, P. Zheng, Q. Wang, W. Chen, H. Jin, and D. Macdonald, "Recombination sources in p-type high performance multicrystalline silicon," *Jpn. J. Appl. Phys.*, vol. 56, pp. 08MB16-1-16, 2017.

[23] H. C. Sio and D. Macdonald, "Direct comparison of the electrical properties of multicrystalline silicon materials for solar cells: conventional p-type, n-type and high performance p-type," *Sol. Energy Mater. Sol. Cells*, vol. 144, pp. 339 - 346, 2016.

[24] S. Castellanos, K. E. Ekstrøm, A. Autruffe, M. A. Jensen, A. E. Morishige, J. Hofstetter, P. Yen, B. Lai, G. Stokkan, C. del Cañizo, and T. Buonassisi, "High-performance and traditional multicrystalline silicon: comparing gettering responses and lifetime-limiting defects," *IEEE J. Photovolt.*, vol. 6, no. 3, pp. 632-640, 2016.

[25] A. Bentzen, A. Holt, R. Kopecek, G. Stokkan, J. S. Christensen, and B. G. Svensson, "Gettering of transition metal impurities during phosphorus emitter diffusion in multicrystalline silicon solar cell processing," *J. Appl. Phys.*, vol. 99, no. 9, pp. 093509-1-6, 2006.

[26] S. M. Myers, M. Seibt, and W. Schröter, "Mechanisms of transition-metal gettering in silicon," *J. Appl. Phys.*, vol. 88, pp. 3795-3819, 2000.

[27] R. Søndenå, H. Haug, A. Song, C.-C. Hsueh, and J. O. Odden, "Resistivitiy profiles in multicrystalline silicon ingots featuring gallium co-doping," *AIP Conference Proceedings*, vol. 1999, pp. 130016-1-6, 2018.

[28] W. Kern, "The evolution of silicon wafer cleaning technology," *J. Electrochem. Soc.*, vol. 137, no. 6, pp. 1887-1892, 1990.

[29] Z. Hameiri, N. Borojevic, L. Mai, N. Nandakumar, K. Kim, and S. Winderbaum, "Low-absorbing and thermally stable industrial silicon nitride films with very low surface recombination," *IEEE J. Photovolt.*, vol. 7, no. 4, pp. 996-1003, 2017.

[30] H. Li, F. Ma, Z. Hameiri, S. Wenham, and M. Abbott, "An advanced qualitative model regarding the role of oxygen during POCl3 diffusion in silicon.," *Phys. Status Solidi Rapid Res. Lett.*, vol. 11, pp. 1700046-1-4, 2017.

[31] H. Li, F. Ma, Z. Hameiri, S. Wenham, and M. Abbott, "On elimination of inactive phosphorus in industrial POCl3 diffused emitters for high efficiency silicon solar cells," *Sol. Energy Mater. Sol. Cells*, vol. 171, pp. 213-221, 2017.

[32] S. T. Kristensen, S. Nie, M. S. Wiig, H. Haug, C. Berthod, R. Strandberg, and Z. Hameiri, "A high-accuracy calibration method for temperature dependent photoluminescence imaging," *AIP Conference Proceedings*, vol. 2147, pp. 020007-1-6, 2019.

[33] R. Dumbrell, M. K. Juhl, T. Trupke, and Z. Hameiri, "Extracting metal contact recombination parameters," *IEEE J. Photovolt.*, vol. 8, no. 6, pp. 1413-1420, 2018.

[34] J. A. Giesecke, M. C. Schubert, B. Michl, F. Schindler, and W. Warta, "Minority carrier lifetime imaging of silicon wafers calibrated by quasi-steady-state photoluminescence," *Sol. Energy Mater. Sol. Cells*, vol. 95, no. 3, pp. 1011-1018, 2011.

[35] F. Schindler, M. Forster, J. Broisch, J. Schön, J. Giesecke, S. Rein, W. Warta, and M. C. Schubert, "Towards a unified low-field model for carrier mobilities in crystalline silicon," *Sol. Energy Mater. Sol. Cells*, vol. 131, pp. 92-99, 2014.

[36] S. Bernardini, Efficiency-Limiting Recombination Mechanisms in High-Quality Crystalline Silicon for Solar Cells, PhD dissertation, Arizona State Univeristy, 2018.

[37] H. C. Sio, S. P. Phang, T. Trupke, and D. Macdonald, "Impact of phosphorous gettering and hydrogenation on the surface recombination velocity of grain boundaries in p-type multicrystalline silicon," *IEEE J. Photovolt.*, vol. 5, pp. 1357-1365, 2015.

[38] L. J. Geerligs, Y. Komatsu, I. Rover, K. Wambach, I. Yamaga, and T. Saitoh, "Precipitates and hydrogen passivation at crystal defects in n- and p-type multicrystalline silicon," *J. Appl. Phys.*, vol. 102, no. 9, p. 093702, 2007.

[39] J. Chen, T. Sekiguchi, D. Yang, F. Yin, K. Kido, and S. Tsurekawa, "Electron-beam-induced current study of grain boundaries in multicrystalline silicon," *J. Appl. Phys.*, vol. 96, no. 10, pp. 5490-5495, 2004.

[40] D. Macdonald, A. Cuevas, A. Kinomura, Y. Nakano, and L. J. Geerligs, "Transition-metal profiles in a multicrystalline silicon ingot," *J. Appl. Phys.*, vol. 97, pp. 033523-1-7, 2005.

[41] G. Stokkan, Y. Hu, Ø. Mjøs, and M. Juel, "Study of evolution of dislocation clusters in high performance multicrystalline silicon," *Sol. Energy Mater. Sol. Cells*, vol. 130, pp. 679-685, 2014.

[42] W. Shockley and W. T. J. Read, "Statistics of the recombination of holes and electrons," *Phys. Rev.*, vol. 87, no. 5, pp. 835-842, 1952.

[43] R. N. Hall, "Electron-hole recombination in germanium," *Phys. Rev.*, vol. 87, p. 387, 1952.

[44] Z. Hameiri, M. K. Juhl, R. Carlaw, and T. Trupke, "Spatially resolved lifetime spectroscopy from temperature-dependent photoluminescence imaging," in: *42nd IEEE Photovoltaic Specialist Conference*, New Orleans, LA, 2015.

[45] S. Rein, *Lifetime Spectroscopy: A Method of Defect Characterization in Silicon for Photovoltaic Applications*, Springer, 2005.

[46] B. B. Paudyal, K. R. McIntosh, and D. Macdonald, "Temperature dependent electron and hole capture cross sections of iron-contaminated boron-doped silicon," in: *34th IEEE Photovoltaic Specialists Conference*, Philadelphia, PA, 2009.

[47] A. Inglese, J. Lindroos, H. Vahlman, and H. Savin, "Recombination activity of light-activated copper defects in p-type silicon studied by injection- and temperature-dependent lifetime spectroscopy," *J. Appl. Phys.*, vol. 120, pp. 125703-1-8, 2016.

[48] J. Schmidt, "Temperature- and injection-dependent lifetime spectroscopy for the characterization of defect centers in semiconductors," *Appl. Phys. Lett.*, vol. 82, no. 13, pp. 2178-2180, 2003.

[49] B. B. Paudyal, K. R. McIntoch, D. H. Macdonald, and G. Coletti, "Temperature dependent carrier lifetime studies of Mo in crystalline silicon," *J. Appl. Phys.*, vol. 107, no. 5, pp. 124510-1-5, 2010.

[50] B. B. Paudyal, K. R. McIntosh, and D. H. Macdonald, "Temperature dependent carrier lifetime studies on Ti-doped multicrystalline silicon," *J. Appl. Phys.*, vol. 105, pp. 124510-1-5, 2009.

[51] J. Schmidt, R. Krain, and K. Bothe, "Recombination activity of interstitial chromium and chromium-boron pairs in silicon," *J. Appl. Phys.*, vol. 102, pp. 123701-1-10, 2007.